JOURNAL OF GEOPHYSICAL RESEARCH, VOL. 106, NO. E3, PAGES 5099–5105, MARCH 25, 2001

A high-resolution, three-dimensional model of Jupiter's Great Red Spot

James Y-K. Cho,[1,2] Manuel de la Torre Juárez,[3,4] Andrew P. Ingersoll,[1] and David G. Dritschel[5]

Abstract. The turbulent flow at the periphery of the Great Red Spot (GRS) contains many fine-scale filamentary structures, while the more quiescent core, bounded by a narrow high-velocity ring, exhibits organized, possibly counterrotating, motion. Past studies have neither been able to capture this complexity nor adequately study the effects of vertical stratification $L_R(z)$ on the GRS. We present results from a series of high-resolution, three-dimensional simulations that advect the dynamical tracer, potential vorticity. The detailed flow is successfully captured with a characteristic value of $L_R \approx 2000$ km, independent of the precise vertical stratification profile.

1. Introduction

Voyager's and Galileo's reconnaissances transformed our picture of the dynamical character of Jupiter's Great Red Spot (GRS). The high-resolution images returned by the spacecrafts revealed associated motions involving an enormous range of scales: the GRS is a coherent, synoptic-scale ($\sim 10^4$ km) vortex rotating in a region of highly turbulent, fine-scale filamentary cloud structures (Plate 1). The images also revealed that the most dynamic region of the vortex, defined by a steep velocity gradient, is concentrated in a very narrow band at its perimeter. (For vector and streamfield plots of the GRS, see Figures 2 and 3, respectively, of *Dowling and Ingersoll* [1988]; see also *Vasavada et al.* [1998].) Such strong, sharp gradients bounding a vortex are not unique in planetary atmospheres. For example, Earth's wintertime stratospheric polar vortices are bounded by similarly steep gradients [*Juckes and McIntyre,* 1987]. For the Earth's atmospheric vortices, it has long been recognized that a crucial requirement in understanding the detailed flow structure is the ability of numerical models to resolve the fine scales.

In this paper we summarize the results from a series of high-resolution, three-dimensional (3-D) numerical simulations of Jupiter's GRS and its environs. A well-tested method, which advects the materially conserved potential vorticity, is employed [*Dritschel and Ambaum,* 1997]. Note that both potential vorticity (PV) and clouds serve as dynamical tracers. Tracer fields possess much greater small-scale structures than either the velocity or the stream field, allowing a more detailed comparison to be made against observations. Note also that because of the invertibility principle of PV [*Hoskins et al.,* 1985], the velocity vectors are roughly tangent to the PV.

In the past, 2-D (1- or $1\frac{1}{2}$-layer) numerical simulations have been used, primarily focusing on the spot's dynamical origin and survivability [*Williams,* 1985; *Marcus,* 1988; *Dowling and Ingersoll,* 1989; *Cho and Polvani,* 1996]. These studies have shown that despite their simplicity, single shallow-layer atmospheric dynamics models can successfully explain the longevity of the GRS under a variety of Jovian-like conditions.

However, because of their limited horizontal resolution, those studies were unable to capture the detailed features of the complex flow observed within and around the GRS. In particular, in addition to the high-gradient band or ring feature mentioned above, some of the features in Plate 1 previously not captured are: (1) the possibly organized, medium-scale ($\sim$1000 km) structures at the core of the GRS; (2) the strong southward bending of the westward flow immediately to the north of the GRS; (3) the undulating filament trailing to the northeast of the GRS; and (4) the fine-scale filamentary structures at the periphery of the vortex, which partially wrap around the GRS, giving its "cuspy" sides. In addition, the full effects of atmospheric stratification, characterized by the Brunt-Väisälä (buoyancy)

[1]Division of Geological and Planetary Sciences, California Institute of Technology, Pasadena, California.

[2]Now at Spectral Sciences, Inc., Burlington, Massachusetts.

[3]Jet Propulsion Laboratory/National Research Council, Pasadena, California.

[4]On leave from ETSI Aeronáuticos, Universidad Politécnica de Madrid, Spain.

[5]Mathematical Institute, University of St. Andrews, Scotland.

Copyright 2001 by the American Geophysical Union.

Paper number 2000JE001287.
0048-0227/01/2000JE001281$9.00

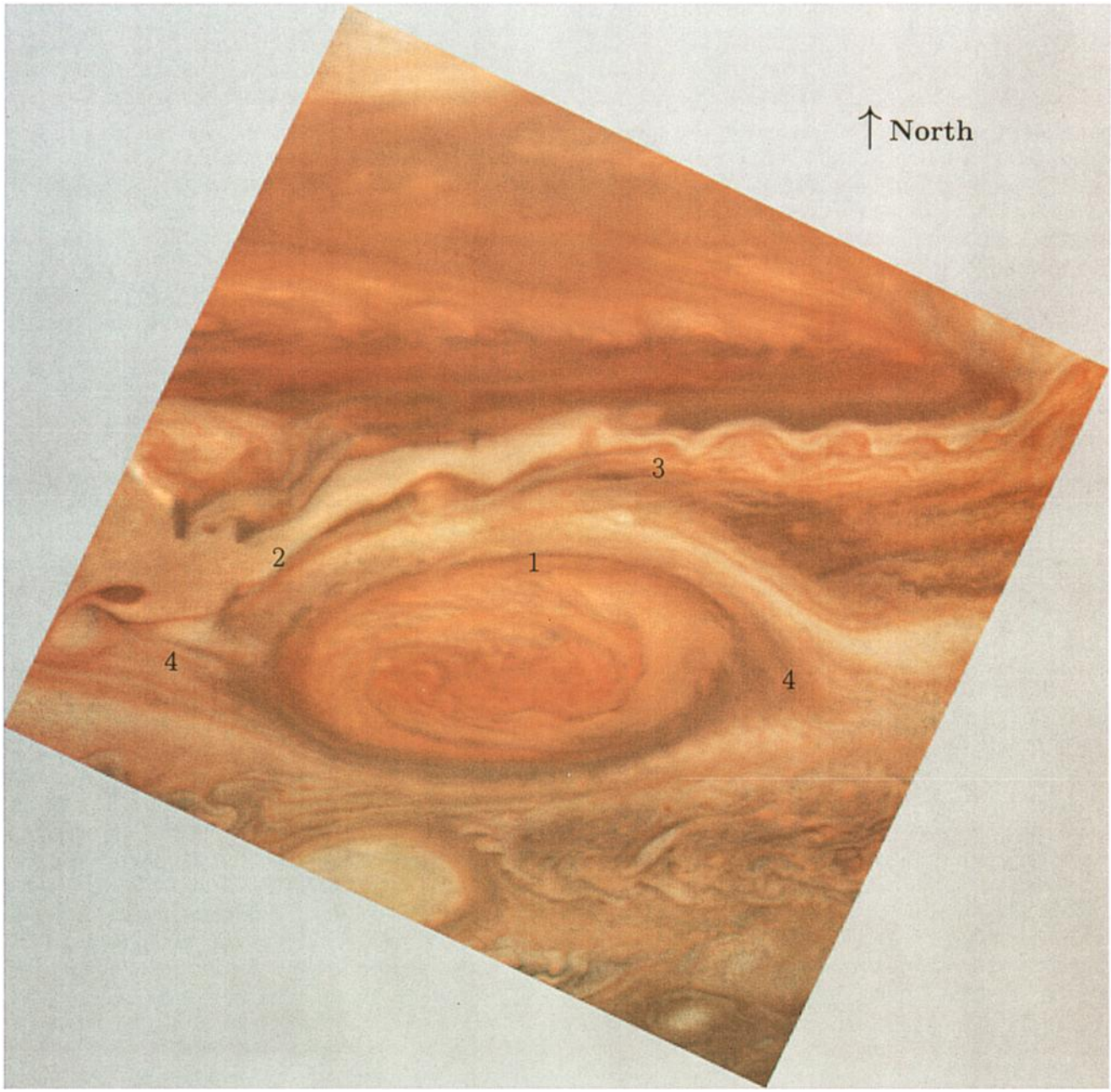

Plate 1. Jupiter's Great Red Spot (GRS): a mosaic from Voyager, with orientation as indicated. The GRS is characterized by (1) a high-velocity ring feature demarcating its boundary and medium-scale structures at the core; (2) a strong southward bending of westward flow at the northwestern side; (3) trailing undulations to the northeast; and (4) the fine-scale filamentary structures at the periphery of the vortex, giving a "cat's eye" shape.

frequency, on the GRS were not studied since a high vertical resolution (many layers) is necessary for such a study. Only recently, two simulations with more than one vertical degree of freedom have been performed [*Achterberg and Ingersoll,* 1989; *Williams,* 1997]. However, they still lacked the horizontal resolution to capture the mentioned features of interest or to study the detailed effects of the Brunt-Väisälä frequency on the flow in and around the GRS.

2. Model

In this work we model the region of the atmosphere in which the GRS can be followed with visible (cloud and haze) tracers. This region is stably stratified and rapidly rotating; hence the motion is predominantly layer-wise. Therefore we use the quasi-geostrophic (QG) approximation [*Pedlosky,* 1979], appropriate for any synoptic-scale structure on timescales much shorter than the diabatic warming or radiative cooling times. The governing equation expresses the material conservation and transport of PV, q:

$$\frac{Dq}{Dt} \equiv (\frac{\partial}{\partial t} + \mathbf{v}\cdot\nabla)\, q = 0, \qquad (1)$$

where

$$q = f + \nabla^2\psi + \frac{1}{\rho_0}\frac{\partial}{\partial z}(\rho_0 \frac{f_0^2}{N^2}\frac{\partial \psi}{\partial z}) + \Xi. \qquad (2)$$

In (1), $\mathbf{v} = (u, v) = (-\partial\psi/\partial y, \partial\psi/\partial x)$ is the horizontal velocity, where $\psi = \psi(x, y, z, t)$ is the streamfunction. In (2), ∇^2 is the horizontal Laplacian; $f = f_0 + \beta y$ is the Coriolis parameter, with β being the planetary vorticity gradient. $\Xi = \gamma(x, y, t)\delta(z)$ is the equivalent sheet contribution to the PV by the generally inhomogeneous boundary condition [*Hoskins et al.,* 1985] at the bottom ($z = 0$), with $D\gamma/Dt = 0$ and $\delta(z)$ being a Dirac delta function. Also, $\rho_0(z)$ and $N(z)$ are the basic-state density and the Brunt Väisälä profiles, respectively, in log-pressure coordinate z. The description and extensive tests of the numerical algorithm used to solve the governing equation are presented by *Dritschel and Ambaum* [1997].

3. Results

The typical results from our numerical simulations are shown in Figures 1 and 2. Although much of the computed detail far exceeds the resolution capacity of the graphics (and hence is only partially rendered in the figures), the 3-D flow field when plotted is still quite complex. Therefore the view from the top is presented for clarity and the PV contours in the lower layers are shown as dashed lines. (In the cases shown here, the flow is vertically very uniform.) In all the simulations, the computational domain is doubly periodic on the sides (of $2\pi \times 10^4$ km each) with a flat bottom ($\partial\psi/\partial z = 0$, $\gamma = 0$) and a free surface ($\partial\psi/\partial z + N^2\psi/g = 0$) at the top ($z = 1.25H_s$, where H_s is the density scale height). The latter boundary condition is general and reduces to the traditional "rigid-lid" approximation ($\partial\psi/\partial z \to 0$) for a weakly stratified atmosphere ($N \to 0$).

In Figure 1, an eight-layer (eight vertical modes) simulation is shown at two different times; we have performed calculations with up to 60 layers and have verified that the results presented here do not change qualitatively with higher vertical resolution. Here, $N(z) = N^* z$, where $N^* = cN_s$ with c being a constant and $N_s \equiv (g^2/T_s c_p)^{1/2} = 0.017$ s^{-1}, using the standard Jupiter values [*Ingersoll,* 1990] of $g = 22.9$ m s^{-2}, $c_p = 13213$ m^2 s^{-2} K^{-1}, and $T_s = 140$ K. The density scale height, $H_s \equiv RT_s/g$, is 23.1 km with $R = 3779.1$ m^2 s^{-2} K^{-1}; the characteristic Rossby deformation radius, $L_R{}^* \equiv N^* H_s/f_0$, is 2000 km with $f_0 = 4\pi \sin(-22.5)/35740$ s^{-1} $= 1.3\times10^{-4}$ s^{-1}; and the relative density and pressure profiles are $\rho(z)/\rho(0) = p(z)/p(0) = \exp(-z/H_s)$. The simulation time unit, $t = 1$, corresponds to 0.2 Jovian days, or ~0.1 GRS turnaround times; a fourth-order accurate Runge-Kutta scheme is used for the time stepping.

The common initial configuration for all the cases discussed in this work is shown in Figure 1a. In the domain, uniform areas of PV are contoured by lines, which are advected by the flow. Thus the lines serve as flow tracers. The GRS is initially specified as an elliptical column of uniform relative vorticity ($q - f$), centered at $-22.5°$ with semimajor and semiminor diameters of 2×10^4 and 1×10^4 km, respectively. The column is "embedded" (In the observations, as well as in our simulations, the GRS "overfills" the jets.) in a pair of barotropic (z-independent) E-W jets: one westward at $-20°$ latitude and the other eastward at $-28°$ latitude. A jet here is composed of two uniform strips of PV, with each strip representing an edge (equatorward or poleward) of the jet and the jump between them corresponding to the jet core (extremum); the size and strength of a jet is related to the width of the strips and the jump value between them. In our simulations a series of strips and jumps is chosen to initially match the zonal (E-W) jets presented by *Limaye* [1986], as well as the planetary vorticity gradient, at the latitudes near the GRS. The resulting flow is due to the combined contributions from the vortex, the jets, and the planetary rotation.

The situation is similar to that in several past simulations. However, unlike in those studies, the jets in our study more accurately represent the observed flow near the GRS, deflecting from their respective latitudes and bending around the vortex column as they zonally traverse the domain (See, for example, the line immediately north of the ellipse, which spans E-W all the way across the domain.). Note also that the dynamical structures in our simulations (vortex and jets) interact and evolve freely, without being subject to the influence of externally imposed conditions (e.g., uniform shear or bottom topography): the evolution, including any baroclinicity that develops, is strictly due to the

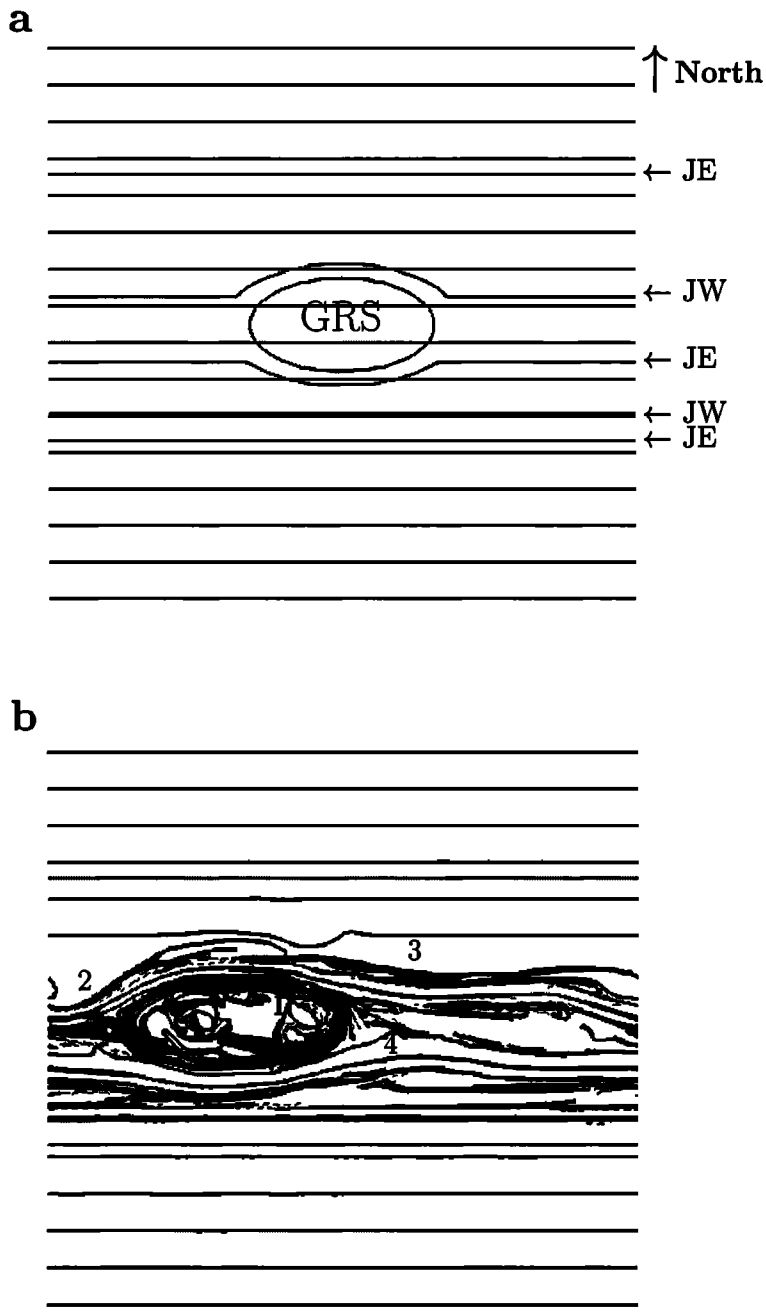

Figure 1. Potential vorticity isocontours from an eight-layer simulation with $N(z) = N^* z$ such that $L_R^* \approx 2000$ km: (a) $t = 0$ and (b) $t = 533$, where $t = 1$ corresponds to ~0.1 GRS turnaround times. The field is a superposition of the individual vorticity contributions from the vortex ("GRS"), the jets ("JE" and "JW," indicating position of eastward and westward jet maxima, respectively), and the planetary vorticity gradient (equally spaced unmarked horizontal lines). Areas of constant potential vorticity are demarcated with material lines, which subsequently move with the flow as tracers. The top view is shown. The flow in Figure 1b, which evolved starting from the configuration in Figure 1a, very realistically resembles the observation (compare with Plate 1): the shape, stability, and fine-scale filamentary structures, as well as the core motion, are all captured in this simulation. There is no qualitative difference in the flow pattern at $t = 2000$ or with the sixty-layer vertical resolution.

nonlinear interaction between the free structures in the flow. The important effects of imposed, dynamic (i.e., time-dependent) bottom boundary conditions, arising from the neutrally stable motion from below, will be reported elsewhere.

Starting with the initial condition depicted in Figure 1a, the evolution after 533 time units (~53 GRS rotations) is shown in Figure 1b. By comparing Figure 1b with Plate 1, it can be seen that numerous detailed features in the latter, not obtained in previous simulations,

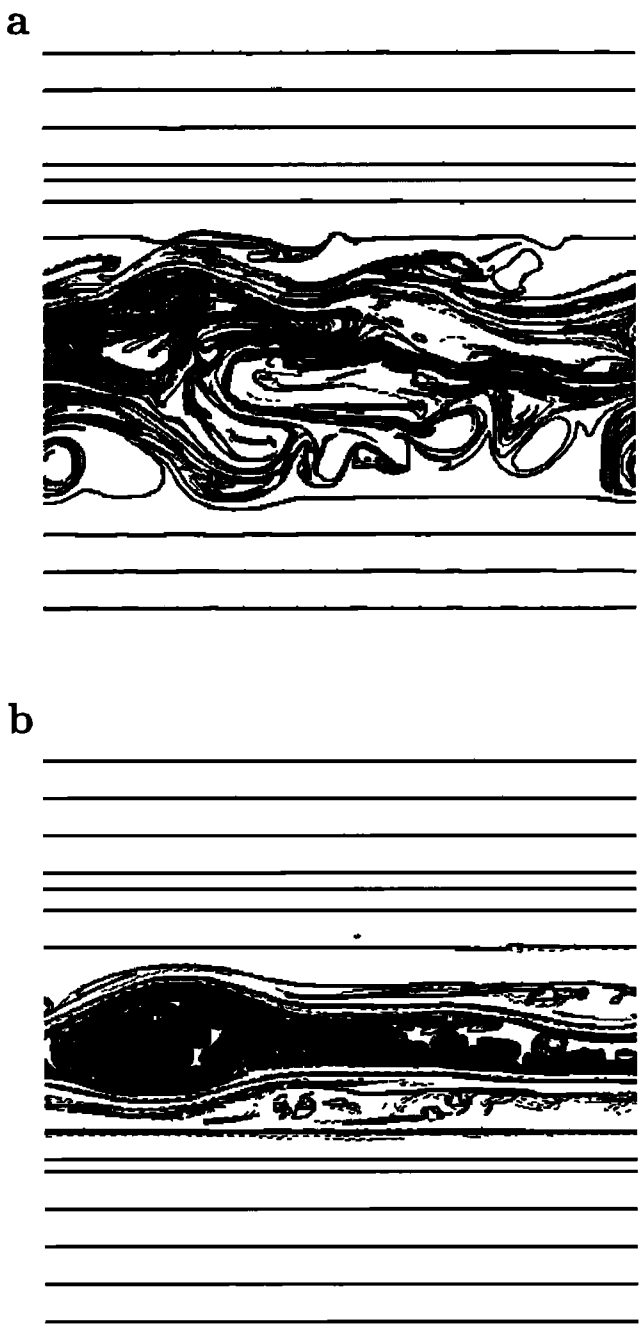

Figure 2. Potential vorticity isocontours from two different simulations with all parameters identical to those of Figure 1, except N^*, which is (a) twice and (b) half of that in Figure 1b. The flow fields at (a) $t = 360$ and (b) $t = 3300$ are shown; the initial configurations for both simulations are as in Figure 1a. The N^* (and hence $L_R{}^*$) values in both simulations lead to unstable or incoherent GRS, in direct contrast to the observations; thus they are not the appropriate values for the GRS.

are realistically captured in this simulation. First, thin filaments are formed and advected around the elliptical vortex column, tracing a cuspy "cat's eye" flow pattern, which resembles very closely the actual flow around the GRS. Second, the initial E-W symmetry of the flow is clearly broken as the westward flow north of the GRS is substantially pulled southward at the northwestern side of the vortex. Third, a tight ring of high PV gradient (bundle of PV lines) is formed, capturing the familiar, characteristic "collar" of the GRS. In both the simulation and the observations, the ring corresponds to a well-organized circulating region of high velocity in the flow.

In QG dynamics, such a sharp feature is a natural consequence of a small L_R (small compared to the size of the vortex); here, L_R varies linearly from 0 km at the bottom to 2000 km at the top. Another consequence is the relatively quiescent (compared to the ring) vortex center, where there is a notable absence of comparably large-scale, organized structure. Instead, the center contains smaller-scale (~1000 km) coherent structures, which slowly counter rotate with respect to the outer ring (Figure 1b), as reported in recent Galileo observations [*Vasavada et al.*, 1998]. We also note here a small amount of baroclinicity ($\partial \mathbf{v}/\partial z$) in the flow (exhibited by the dashed lines) due to the strong stratification. The flow is, in general, barotropic (vertically coherent), as in Voyager and Galileo observations. A longer time integration (of up to $t = 2000$) shows the vortex to be stable and the overall flow to be not too different from that in Figure 1b, except for a westward translation due to drift caused by the β effect.

For an atmosphere in hydrostatic equilibrium with vertical temperature profile $T = T(z)$ and lapse rate $\partial T/\partial z$, the buoyancy frequency profile

$$N(z) = \sqrt{\frac{g}{T}\left(\frac{\partial T}{\partial z} + \frac{g}{c_p}\right)}. \tag{3}$$

The $N(z) = N_s\phi(z)$ profile used in the simulation of Figure 1b, where $\phi(z)$ is an arbitrary function, is based on the temperature profiles obtained by the Voyager radio occultation measurements [*Lindal et al.*, 1981] and is similar to a previously used profile [*Achterberg and Ingersoll*, 1989]. The only other data (from the Galileo probe) show that the lapse rate is close to zero but subadiabatic down to 24 bar pressure level [*Seiff et al.*, 1996]. Hence we have varied the vertical stratification profile using several different functional forms. In our simulations we have observed that the evolution is not critically sensitive to the precise functional form (e.g., linear, quadratic, exponential, or even constant) of the $N(z)$ profile in the modeled height range. It is, however, very strongly sensitive to the maximum value of $N(z)$, clearly establishing the dynamically significant role of N^* (and hence $L_R{}^*$) for the GRS and its surrounding region on Jupiter. Note that the uncertain moisture content of Jupiter's atmosphere most strongly affects the stability structure far below the visible cloud deck and, given our results, is not expected to play a significant, stabilizing dynamical role.

The role of L_R in geophysical-astrophysical fluid dynamics is well known. Of particular interest here is its ability to screen and reduce the interaction strength between the flow structures. The GRS and the background jets are shielded from their mutual interaction

approximately exponentially fast with their separation distance. In addition, it has been recently shown that a QG vortex column of height-to-width ratio δ less than roughly $3f_0/N = 3H_s/L_R$ (here, $\delta \sim 0.001$ and $3f_0/N \sim 0.01$) in a horizontal straining field is baroclinically stable to 3-D disturbances [*Dritschel and de la Torre Juárez,* 1996]. That is, a weakly interacting, coherent shallow vortex column is both horizontally and vertically stable: hence the localized, coherent, and predominantly barotropic look of the flow in Figure 1b, and, we believe, the GRS. To illustrate this point further, the dynamical responses to variations in N^* are shown in Figure 2.

Figure 2a shows the behavior for a case with all simulation parameters identical to those of Figure 1b, except with $N^* \rightarrow 2N^*$. The characteristic Rossby deformation radius L_R^* is now 4000 km. The flow is shown at $t = 360$, or ~36 GRS rotations. Initially, the evolution for this case is similar to that in Figure 1b. However, because of to the increase in the interaction length, the vortex is no longer weakly interacting, and the evolution is much more dynamic in this case. After a brief "similar" period (at $t \approx 250$) the jet-vortex system quickly and violently becomes unstable, as shown in Figure 2a. Most notably, the vortex begins to precess and eventually splits the bottom eastward jet, deflecting part of it southward on the west side of the GRS and northward on the east side. Afterward, the two deflected streams suffer Kelvin-Helmholtz instability (large undulations of the PV due to adverse horizontal shear, $\partial q/\partial y$), and vertical sheets of PV roll up into many vortex columns south of the GRS. This is contrary to observations. In addition, unlike in the previous case, the core always corotates with the outer ring; hence no counterrotating motion is observed in this case. The only common feature with the previous case is that the evolution is again quite barotropic, even after a long time; only in the passive (weak), thin filaments are there signs of baroclinicity.

Figure 2b shows the behavior for a case with all simulation parameters identical to those of Figure 1b, except with $N^* \rightarrow N^*/2$. Therefore L_R^* is now 1000 km. The flow is shown at $t = 3300$, or ~330 GRS rotations. As in Figure 2a, the flow is again markedly different than that shown in Figure 1b. In this case the vortex is not coherent. There is an immediate and severe vortex wave breaking in the northwestern sector of the vortex, and weak trailing vortices and tangles of filaments form later east of the vortex. Most notably, the PV in the latitude band in which the vortex was initially located eventually becomes very well-homogenized, to the point that the "GRS" is now even difficult to detect (Figure 2b). This means that none of the characteristic features of the GRS, such as the ring, is present. As discussed earlier, this loss of coherence is due to the small interaction length L_R as a consequence, the vortex cannot maintain its shape as it effectively loses the ability to "feel" the other side of itself. In addition, for a long time (~1000 time units), there is no core motion at all. These behaviors are all again contrary to observations. As expected, we have observed that the loss of coherence is even more pronounced in the cases with smaller N^*, in which the "GRS" completely fails to maintain its oval shape and is simply smeared out into a band. Although both of the behaviors in Figure 2 are permissible solutions of the QG equation, they are not observed on Jupiter. Hence the most likely $N(z)$ profile for the GRS is the one used in the case of Figure 1b.

4. Summary

In conclusion, following *Marcus* [1988] and *Achterberg and Ingersoll* [1994], we have used QG dynamics to model Jupiter's GRS. Here we have extended the previous studies by performing our simulations with unconstrained structures and with much greater horizontal and vertical resolutions, allowing us to investigate in detail the hydrodynamic stability and shape of the GRS. Since the actual vertical structure of the atmosphere ($L_R(z)$) at the GRS region is not known, we have assumed several representative structure profiles and found that the 3-D flow is very sensitive to the characteristic value of the deformation radius L_R^* (while less sensitive to the precise functional dependence on z): the case with $L_R^* \approx 2000$ km gives realistic-looking flows, while the cases with ~4000 km and ~1000 km do not. The 2000 km value is consistent with the vertical structure profile obtained by *Lindal et al.* [1981] for several locations on Jupiter away from the GRS region, suggesting that that profile may be more representative of the entire planet. Our simulations show that although physically simple, the QG model can capture very accurately the highly complex flow patterns revealed in Voyager and Galileo images as well as tightly constrain and identify the crucial aspects of the vertical structure of the region in and around the GRS.

Acknowledgments. J. Y-K. C. and A. P. I. were supported by NASA's Planetary Atmospheres Program; M. T. J. was supported by NASA/N.R.C.; and D. G. D. was supported by N.E.R.C. We thank Ashwin Vasavada and Adam Showman for helpful discussions and the reviewers for helpful suggestions.

References

Achterberg, R. K., and A. P. Ingersoll, A normal-mode approach to Jovian atmospheric dynamics, *J. Atmos. Sci., 6,* 2448-2462, 1989.

Achterberg, R. K., and A. P. Ingersoll, Numerical simulation of baroclinic Jovian vortices, *J. Atmos. Sci., 51,* 541-562, 1994.

Cho, J. Y-K., and L. M. Polvani, The morphogenesis of bands and zonal winds in the atmospheres of the giant outer planets, *Science, 273,* 335-337, 1996.

Dowling, T. E., and A. P. Ingersoll, Potential vorticity and layer thickness variations in the flow around Jupiter's Great Red Spot and White Oval BC, *J. Atmos. Sci., 45,* 1380-1396, 1988.

Dowling, T. E., and A. P. Ingersoll, Jupiter's Great Red

Spot as a shallow-water system, *J. Atmos. Sci., 46,* 3256-3278, 1989.

Dritschel, D. G., and M. H. P. Ambaum, A contour-advective semi-Lagrangian algorithm for the simulation of fine-scale conservative fields, *Q. J. R. Meteorol. Soc., 123,* 1097-1130, 1997.

Dritschel, D. G., and M. de la Torre Juárez, The instability and breakdown of tall columnar vortices in a quasi-geostrophic fluid, *J. Fluid Mech., 328,* 129-160, 1996.

Hoskins, B. J., M. E. McIntyre, and A. W. Robertson, On the use and significance of isentropic potential-vorticity maps, *Q. J. R. Meteorol. Soc., 111,* 877-946, 1985.

Ingersoll, A. P., Atmospheric dynamics of the outer planets, *Science, 248,* 308-315, 1990.

Juckes, M. N., and M. E. McIntyre, A high resolution, one-layer model of breaking planetary waves in the stratosphere, *Nature, 328,* 590-596, 1987.

Limaye, S. S., Jupiter: New estimates of the mean zonal flow at the cloud level, *Icarus, 65,* 335-352, 1986.

Lindal, G. F., et al., The atmosphere of Jupiter: An analysis of the Voyager radio occultation measurements, *J. Geophys. Res., 86,* 8721-8727, 1981.

Marcus, P. S., Numerical-simulation of Jupiter's Great Red Spot, *Nature, 331,* 693-696, 1988.

Pedlosky, J. *Geophysical Fluid Dynamics,* 2nd Ed., Springer-Verlag, New York, 1979.

Seiff, A., et al., Structure of the atmosphere of Jupiter: Galileo probe measurements, *Science, 272,* 844-845, 1996.

Vasavada A. R., et al., Galileo imaging of Jupiter's atmosphere: The Great Red Spot, equatorial region, and White Ovals, *Icarus, 135,* 265-275, 1998.

Williams, G. P., Jovian and comparative atmospheric modeling, *Adv. Geophys., 28A,* 381-428, 1985.

Williams, G. P., Planetary vortices and Jupiter's vertical structure, *J. Geophys. Res., 102,* 9303-9308, 1997.

J. Y-K. Cho, Spectral Sciences Inc., 99 South Bedford Street, 7, Burlington, MA 01803-5169. (jcho@spectral.com)

M. de la Torre Juárez, M-S 238-600, JPL/Caltech, 4800 Oak Grove Drive, Pasadena, CA 91109. (mtj@jpl.nasa.gov)

D. G. Dritschel, Mathematical Institute, University of St. Andrews, North Haugh, St. Andrews KY16 9SS, Fife, Scotland. (dgd@mcs.st-and.ac.uk)

A. P. Ingersoll, Division of Geological and Planetary Sciences, California Institute of Technology, Pasadena, CA 91125. (api@gps.caltech.edu)

(Received June 5, 2000; revised November 3, 2000; accepted November 27, 2000.)